Simulation of the Electric Signal During the Formation and Departure of Droplets in the Electroslag Remelting Process

A. KHARICHA, M. WU, A. LUDWIG, and E. KARIMI-SIBAKI

In the ESR process, it is very difficult to make experimental observations of the phenomena occurring within the molten slag. At present, the state of the process is solely evaluated from the variation of the measured electric variables. The present paper proposes the use of 3D numerical model to explore the complex coupling existing between the electrodynamics and the phase distribution during the process. The droplet formation during melting of an electrode under the action of a strong DC current is simulated with a multiphase-magnetohydrodynamic approach. A volume-of-fluid approach is used for the interface tracking, and the potential formulation is used to determine the electric and magnetic fields. The Lorentz force and the Joule heating are recalculated at each time step as a function of the phase distribution. The evolution of the electric resistance of the system during the droplet formation and departure is reported. The results are compared with the measurements made in experimental and industrial-scale ESR processes. Two values of metal/slag interfacial tension of 1 and 0.1 N m^{-1} are explored. The effects of the control system as well as the presence of a horizontal magnetic field are also investigated. These results open the possibility to link online the voltage signal variation with real physical phenomena happening during the process.

DOI: 10.1007/s11663-015-0550-4

I. INTRODUCTION

ELECTROSLAG remelting (ESR) is a metallurgical process which combines and couples many phenomena such as magnetohydrodynamics (MHD), heat and mass transfer, and electrochemistry. Due to the use of opaque materials and high temperatures, experimental observation of the process is very difficult. Many fundamental aspects of this process are still unclear and subject of controversy. The process is monitored and controlled mainly through the electric signal measured during melting. It is known that the droplet formation and departure generate a large part of the observed voltage fluctuation (known also as voltage or resistance swing). In addition, the development of heat and mass transfer at the slag/droplet interface is important for the final ingot quality, composition, and cleanliness. The heat transfer from the slag to the liquid pool is largely dominated by the droplets.

In References 1, 2, transparent experimental models were presented in which single droplet departure during melting was observed. The slag was a transparent eutectic LiCl–KCl alloy which was used to remelt electrodes made of metals with low melting temperatures (Pb, Cu, Zn, Al). During melting, the voltage across the slag layer was monitored with an oscilloscope. Figures 1 and 2 represent the typical oscilloscope trace of the voltage during the formation and departure of aluminum droplets. This typical change in electric parameters (voltage or resistance) can then be used to detect the occurrence of a droplet departure in the conventional non-transparent slags. The typical droplet mass was estimated in References 3, 4 by combining the resulting dripping frequency with the melting rate.

Systematic experiments to correlate the dripping frequency with process parameters using non-transparent slags are reported in Reference 4. With the same power input and up to slag height of about 300 mm, the frequency of droplet departure was found to increase with slag height. Almost no change was observed for slag height larger than 300 mm.

Based on the droplet signature as the one measured in Figures 1 or 2, an invention (US Patent 6019811 (2000)[5]) was patented to better predict the melt rate during ESR process. By counting droplets and empirically determining an approximate quantity of metal in each droplet, a melt rate determination can be made over both long and short periods of time.

A. KHARICHA, Senior Scientist, Group Leader, and M. WU, Professor, Group Leader, are with the Christian-Doppler Laboratory on Advanced Process Simulation of Solidification and Melting, Department of Metallurgy, Montanuniversitaet Leoben, 8700 Leoben, Austria, and also with the Chair for Simulation and Modelling of Metallurgical Processes, Department of Metallurgy, Montanuniversitaet Leoben, 8700 Leoben, Austria. Contact e-mail: abdellah.kharicha@unileoben.ac.at A. LUDWIG, Full Professor, is with the Chair for Simulation and Modelling of Metallurgical Processes, Department of Metallurgy, Montanuniversitaet Leoben. E. KARIMI-SIBAKI, Ph.D. Student, is with the Christian-Doppler Laboratory on Advanced Process Simulation of Solidification and Melting, Department of Metallurgy, Montanuniversitaet Leoben.

Manuscript submitted March 20, 2014.
Article published online January 25, 2016.

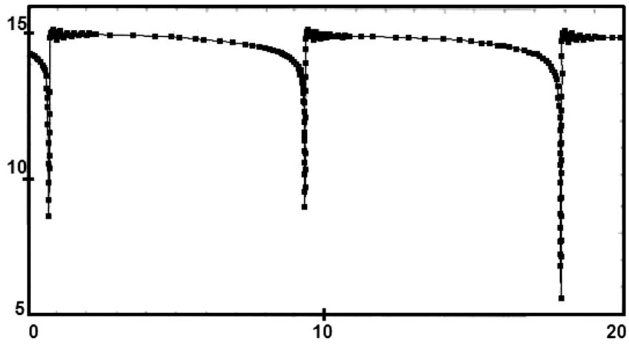

Fig. 1—Experimental cathode ray oscilloscope trace of the voltage (V) across the slag layer during formation and detachment of three aluminum droplets. Picture and caption are taken from Ref. [1]. Note that no axis labels are given in the original.

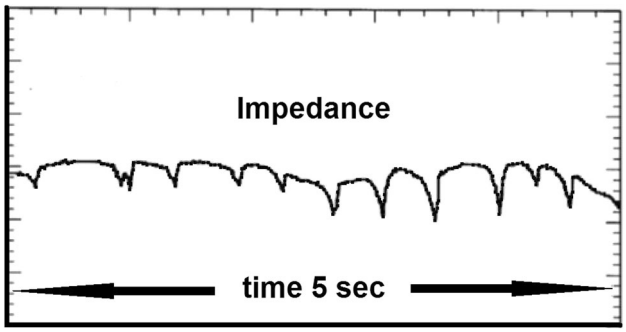

Fig. 2—Exemplary graph of ESR droplet (steel) characteristic waveform in the impedance signal (AC current). Picture and caption are taken from Ref. [5]. Note that no axis labels are given in the original.

Experiments reported in the literature[2,6,7] have also shown that when a magnetic field is applied, deviation of the metallic droplet toward the mold or atomization in much smaller droplets is observed. In industrial process condition, visual observation of the droplet formation just under the electrode being melted is very difficult. This is why no known experiments are reported for industrials scales ESR. The effect of droplets transport on the process was recently studied with computational tools.[8] Usually, the influence of the droplets is essentially taken into account in the form of a momentum and energy sources applied to slag and pool regions.[9–12] Among the other parameters that can exert an influence on the droplet size are the shape of the electrode tip, the slag temperature, the slag composition, and the electric current frequency.[1]

Most industrial ESR processes are running with 50 or 60 Hz of frequency of the applied current. The primary reason to use AC currents is to avoid net electrochemical reactions at the metal/slag interface. However, AC current with applied frequency lower than 1 Hz is generally used to produce large ingots (diam. >1000 mm). The aforementioned electric current can be considered as "quasi DC," since no electrodynamics skin effect can be occurred when a very small frequency is applied. Differences in droplet size were observed between DC negative electrode and DC positive electrode remelting processes.[1,13] The reason for that was assumed to be a change in surface tension as a result of either some electrochemical oxygen transfer from the slag to the metal or to some electro-capillarity phenomena.

The full coupling between the MHD and the multiphase flow fields has been used successfully to solve 2D problems related to the ESR process.[14,15] Furthermore, we extended our 2D models to study the melting and shape of electrode tip.[16,17] Recently, a full scale 3D simulation of the ESR process was performed including the solidification of the ingot.[18] However, the effects of droplets on the global electromagnetic field were ignored.[18] Nevertheless, it is of great importance for fundamental and technical reasons to investigate how the droplet forms and behaves in the slag.

The current work presents the results given by a 3D magnetohydrodynamic model coupled with a volume-of-fluid (VOF) model for the phase's (steel, slag) distribution. During the process, the electrode can develop a flat or a parabolic surface.[17] Here it is assumed to be flat. Due to the high electric resistivity of the slag, it is not a surprise that the electric signal of a droplet fall does not differ between DC and AC ESR operation. The present paper assumes the application of a purely DC current. However, the electric current distribution is dynamically adapted to the transient phase distribution, which means that the overall voltage fluctuates. The electromagnetic forces and the Joule heating are recalculated at each time step. The aim of the present work is to simulate the droplet formation for one specific melting rate. The investigation includes the exploration of the effect of a sudden rise of the imposed electric current intensity, as well as of the presence of a transverse magnetic field.

II. NUMERICAL MODEL

The present analysis chooses a fluid calculation domain that is a cylinder (mold) of $L = 20$ cm in height and $R_1 = 5$ cm in radius. The electrode has a radius of $R_e = 3.5$ cm. The cylindrical container is filled with a column of liquid slag at the top, 17 cm in height, and a quantity of liquid steel at the bottom, 3 cm in height. A solid mold of 5 cm thickness ($R_2 = 10$ cm) surrounding the liquid domain is added aiming to simplify the boundary condition for the magnetic field. The amount of current flows through the fluid domain is known ($I_0 = 1000$ A). Thus, it is considered that equal amount of current is also flowing through the external solid mold, but in the opposite direction. A schematic drawing of the calculation domain is shown in Figure 3. The properties of the steel and slag are given in Table I. The melting rate is set to $M_R = 34$ kg h^{-1}. The properties of steel and slag are assumed to be constant. The electrode supplies a total DC current.

The interface between the molten slag and liquid steel melt is tracked with the geometric reconstruction VOF technique. A single set of momentum equations is shared by the fluids and the volume fraction of each of the fluids in each computational cell is tracked

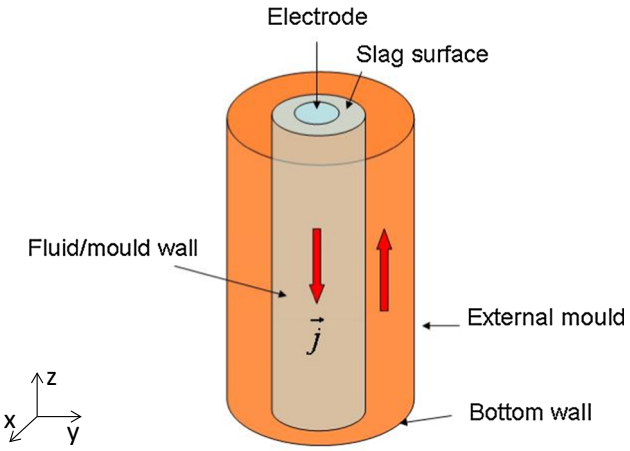

Fig. 3—Schematic drawing of the calculation domain.

Table I. Averaged Material Properties Used for the Calculation

Slag	
Density	2700 kg m^{-3}
Viscosity	0.0025 kg m^{-1} s^{-1}
Electric conductivity	1.2 × 10^2 (Ω m)$^{-1}$
Steel	
Density	6850 kg m^{-3}
Viscosity	0.006 kg m^{-1} s^{-1}
Electric conductivity	7.0 × 10^5 (Ω m)$^{-1}$

throughout the domain. In a two-phase system, the properties appearing in the momentum equation are determined by the presence of the component phase in each control volume. According to the local value of the volume fraction, f_1 for slag and f_2 for the melt, appropriate properties and variables can be assigned to each control volume within the domain. Here, the local values of a physical property such as density ρ, viscosity μ, or electric conductivity σ are linearly interpolated according to the local volume fractions of the slag and melt as

$$\sigma = \sigma_1 f_1 + \sigma_2 f_2,\ \rho = \rho_1 f_1 + \rho_2 f_2 \text{ and } \mu = \mu_1 f_1 + \mu_2 f_2. \quad [1]$$

The value of the interfacial tension between the melt and slag is not precisely known. It is believed to be temperature and electric current dependent. For this numerical study, the value of the interface tension between the melt and the slag is chosen to be equal to 0.1 or 1 N m^{-1}.

A. *Fluid Flow*

The velocity in the liquid phases ($\vec{u}$) is computed from the continuity and the Navier–Stokes equations as follows:

$$\nabla \cdot \vec{u} = 0$$
$$\frac{\partial(\rho\vec{u})}{\partial t} + \nabla \cdot (\rho\vec{u}\vec{u}) = \nabla(\mu\nabla\vec{u}) - \nabla p + \rho\vec{g} + \vec{F}_L \quad [2]$$

where p is the pressure and $\vec{F}_L$ is the Lorentz force. The no-slip condition is applied at the vertical wall (fluid/mold interface). The electrode and the bottom surface are modeled as velocity inlet and outlet.

At the present stage, no reliable multiphase-turbulent model exists that can correctly model the behavior of the turbulence near a liquid–liquid interface. For the liquid/solid boundary, the well-known wall functions were introduced to cope for the presence of the wall boundary layers. Unfortunately, nothing similar exists for liquid–liquid interfaces.

However, some trials were performed in simulating the present process with our available turbulent RANS models. We noticed a diffusion of the turbulent kinetic energy through the metal/slag interface. This is physically incorrect, since the unresolved small eddies cannot cross the phase boundary. Therefore, we did not use any turbulent model at the present stage.

B. *Electromagnetic Field*

The electrodynamic calculation includes the liquid and the mold domains. The well-known $\phi - \vec{A}$ approach[19] is used to estimate the electromagnetic field. It consists of simultaneously solving the electric potential ϕ and the magnetic potential vector $\vec{A}$ equations. The electric potential equation is extracted from the conservation of the electric current as

$$\nabla \cdot \vec{j} = 0 \text{ with } \vec{j} = -\sigma\frac{\partial\vec{A}}{\partial t} - \sigma\nabla\phi. \quad [3]$$

The electric current enters from the electrode and exits the liquid domain from the bottom surface. A flux condition is applied at the bottom surface, while a constant electric potential is applied at the electrode (Table II). This choice is justified by the fact that at the bottom surface, the electric current is more likely to be uniform than at the electrode, where the liquid faucets being formed can considerably deviate the electric current lines. No current is allowed to enter mold wall from the liquid domain. As previously mentioned, it is considered that electric current flows vertically in the upward direction within the solid mold in order to simplify the boundary condition for magnetic vector potential equation. The components are set to

$$\begin{pmatrix} j_x \\ j_y \\ j_z \end{pmatrix} = \begin{pmatrix} 0 \\ 0 \\ \frac{I_0}{\pi(R_2^2 - R_1^2)} \end{pmatrix}. \quad [4]$$

The magnetic potential is related to the magnetic field by

$$\vec{B} = \vec{\nabla} \times \vec{A}. \quad [5]$$

The magnetic induction equation can be formulated in terms of $\vec{A}$ as

$$\nabla \times \left(\frac{1}{\mu_0}\nabla \times \vec{A}\right) = \vec{j}, \quad [6]$$

where μ_0 is the magnetic permeability of vacuum. With the help of Ampere's law, the choice of having a current flowing within the mold in the opposite direction simplifies considerably the external boundary condition for the magnetic potential $\vec{A}$ (Table II). Although the conditions used here correspond to the axisymmetric assumption, the external boundary is far enough to not influence the magnetic field generated around the droplet. The Ampere's law is totally fulfilled by the boundary condition on the vertical wall. Since the same amount of current flows downward and upward, the magnetic field and its potential are zero at the surface of the external cylinder surface. The boundary conditions on the top and the bottom wall express the alignment of magnetic vector potential and the electric current within a cylindrical wire.

The computed electromagnetic field is dynamically adjusted from the space distribution of the electric conductivity, which is in turn function of the predicted phase distribution. The Lorentz force acting on both slag and steel is defined by

$$\vec{F}_{\mathrm{L}} = \vec{j} \times \vec{B}. \qquad [7]$$

The electric resistance can be calculated at each time from the total Joule heating generated in the domain as

$$\mathrm{Res}(t) = \frac{1}{I_0^2} \int \frac{j^2(\vec{x}, t)}{\sigma(\vec{x}, t)} \mathrm{d}\vec{x}^3. \qquad [8]$$

The deviation from the average resistance is defined by

$$\delta\mathrm{Res}(t) = \left(\mathrm{Res}(t) - \frac{1}{2\tau} \int_{-\tau}^{\tau} \mathrm{Res}(t)\mathrm{d}t \right) \Big/ \left(\frac{1}{2\tau} \int_{-\tau}^{\tau} \mathrm{Res}(t)\mathrm{d}t \right), \qquad [9]$$

where τ is an averaging time large enough to include several droplet departures.

Table II. Boundary Conditions

Bottom surface (fluid)	$-\sigma_2 \frac{\partial \varphi}{\partial z} = \frac{I_0}{\pi R_1^2},\ \vec{u} = -\frac{M_R}{\rho_2 \pi R_1^2} \vec{z},\ f_2 = 1$
Electrode	$\varphi = 0,\ \vec{u} = -\frac{M_R}{\rho_2 \pi R_e^2} \vec{z},\ f_2 = 1$
Slag surface	$-\sigma \frac{\partial \varphi}{\partial z} = 0,\ \frac{\partial u_x}{\partial z} = \frac{\partial u_y}{\partial z} = u_z = 0$
Liquid/mold interface	$-\sigma \frac{\partial \varphi}{\partial r} = 0,\ \vec{u} = 0$
Lateral surfaces (mold external)	$\begin{pmatrix} A_r \\ A_\theta \\ A_z \end{pmatrix} = \begin{pmatrix} 0 \\ 0 \\ 0 \end{pmatrix}$
Top and bottom surfaces	$\begin{pmatrix} A_r \\ A_\theta \\ \frac{\partial A_z}{\partial z} \end{pmatrix} = \begin{pmatrix} 0 \\ 0 \\ 0 \end{pmatrix}$

III. CALCULATION PROCEDURE

An iterative segregated procedure was used to solve the set of equations. The equations of the flow, the electric potential, and the magnetic potential were solved. The third-order MUSCL scheme is used for the flow equations discretization. The magnetic potential is discretized with a second-order scheme. The VOF interface is shifted geometrically after the last iteration. A time step corresponding to a courant number of 0.1 was used. Depending on the dynamic of the interfaces, the typical calculation time step lies in the range from 10^{-3} to 10^{-5} seconds. Thanks for using the small time step, 3 to 10 iterations were enough to achieve the convergence of the solution. Grid independence was tested on the convergence of the dripping rate (Table III). The results presented in next sections were obtained with a domain containing about 3.4 million volume elements.

IV. RESULTS AND DISCUSSION

In the following, we distinguish between simulation results where an interfacial tension of 1 N m^{-1} for the slag/metal interface was assumed (Figures 4 through 8), and those assuming a reduced interfacial tension of 0.1 N m^{-1} (Figures 9 and 10).

A. *Interfacial Tension of 1 N m^{-1}*

Figure 4 shows the evolution of the electric current density during the melting of the electrode. The highest current densities are reached when the faucet reaches its maximum length. As the melt is a much better conductor than the molten slag, most of the current provided by the electrode chooses to flow through the metallic path. The computed resistance trace during the formation and detachment of droplets is shown in Figure 5. It can be seen that during the elongation of the metallic faucet (Figures 4(a) through (c)), the electric resistance of system is continuously decreasing. Once the first droplet detaches, the length of the metallic faucet shorten back toward the electrode (Figure 4(d)), and thus the resistance re-increases to stage D. The departure of two small satellite droplets generates two smaller peaks between times D and E. Afterward, although droplets of much smaller size are released, the resistance increases strongly, until the impact of the first droplet on the slag/pool interface occurs (Figure 4(f)). The deformation of the interface in the form of a crater leads to a higher level of the resistance (Figure 4(g)). The interface oscillates for some time before coming back to rest. Another reason for the increase of the resistance is the decrease in volume of the liquid metal previously

Table III. Grid Independence Study Performed on the Case of Fig. 4 (Interfacial Tension of 1 N m^{-1})

Volume elements number (in million)	0.7	1.2	2.1	3.4
Dripping rate (Hz)	1.1	0.88	0.58	0.56

The dripping rate is not constant but fluctuates about 5 pct around the reported values.

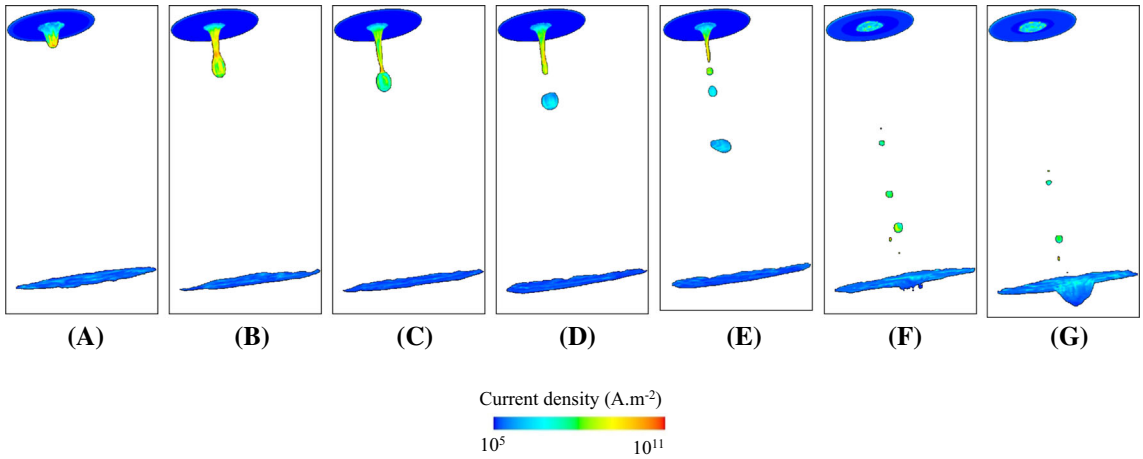

Fig. 4—Views of the slag/metal interfaces colored by electric current density (10^5 to 10^{11} A m^{-2}). (*A*) through (*C*) Formation of the liquid faucet. (*D*, *E*) Droplets formation and detachment. (*F*, *G*) Droplets impacts and deformation of the slag/pool interface.

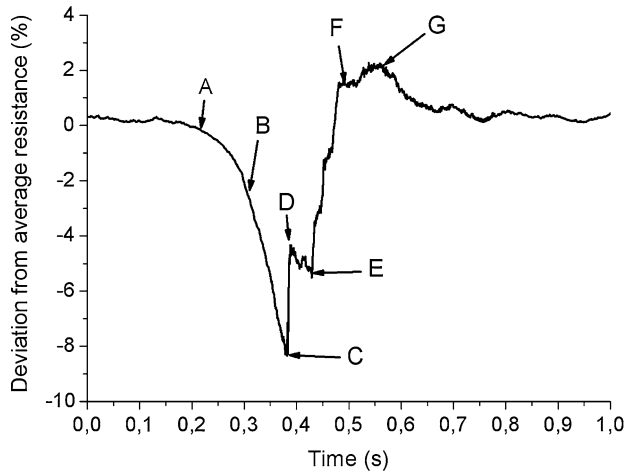

Fig. 5—Detailed evolution of the electric resistance during the droplet formation. The time instants indicated by the letters A to G are related to Fig. 4(A through G).

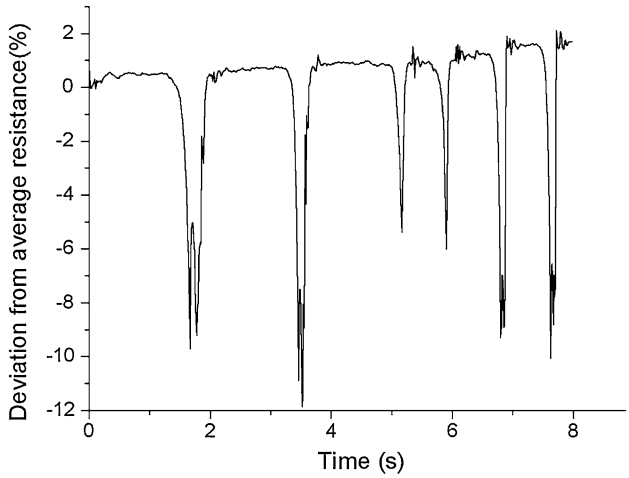

Fig. 6—Fluctuation of the resistance during droplet departure without ($t < 4.5$ s) and with horizontal magnetic field ($t > 4.5$ s).

accumulated under the electrode (Figure 4(a)). This explains why the resistance at $t = 1$ second is slightly higher than at time $t = 0$ second.

Figure 6 shows the evolution of the average resistance deviation during a longer numerical melting experiment. The curve shows several strong variations following the characteristics, as described in Figures 4 and 5. However, each fluctuation is unique considering its amplitude and duration. Although the computation was made for steel, the computed trace during the droplet formation is very similar to that experimental measured in AC or DC current[1,5] (shown in Figures 1 and 2). The typical droplet diameters are of about 10 mm for the larger ones and satellite droplets are of about 1 to 3 mm. The droplet departures occur at a frequency of about 0.6 Hz.

Note that, an additional Lorentz force acts on the liquid (metal and slag) in direction perpendicular to both electric and magnetic fields when an external horizontal magnetic field (0.1*T*) is applied. The presence of an imposed horizontal magnetic field much stronger than the one induced by the vertical current changes the flow patterns. As a consequence of this flow, the droplet is not released from the center of the electrode but at mid distance from the electrode periphery (Figure 7). In the present case, the droplets collided with the lateral wall. This deflection was experimentally observed by Makropoulos *et al.*[2] The presence of the magnetic field increases the droplet departure frequency to almost 1.3 Hz. Since the melting rate is not modified, the droplet at departure is released at shorter distance from the electrode leading to smaller droplet size and smaller minimum peak in the electric resistance signal (Figure 6). In a real system, this increase in dripping frequency was clearly observed in experiments described in Reference 4. Although the power input was the same, an increase of the melting rate of about 20 pct was also noticed. Perhaps this is the results of the strong stirring induced by the imposed magnetic field.

In industrial-scale ESR systems, the induced magnetic field vectors form circles at the electrode. If we consider

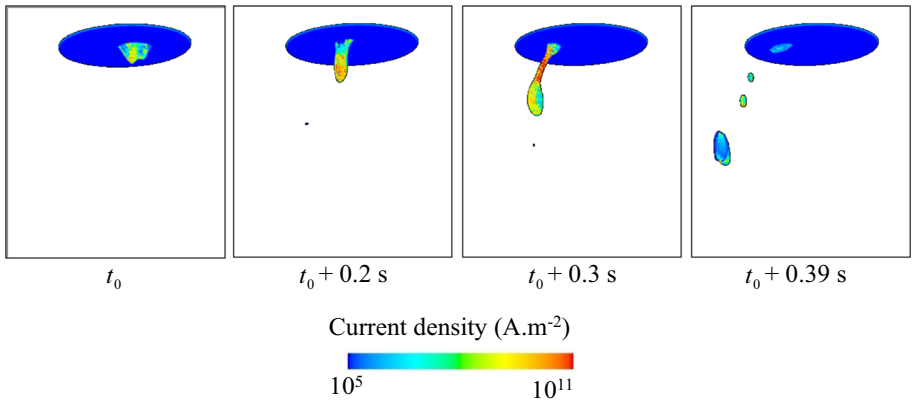

Fig. 7—Droplet formation in the presence of a horizontal magnetic field under the electrode. The main droplet impacts the mold wall. The metal/slag interface is colored with electric current density (10^5 to 10^{11} A m^{-2}).

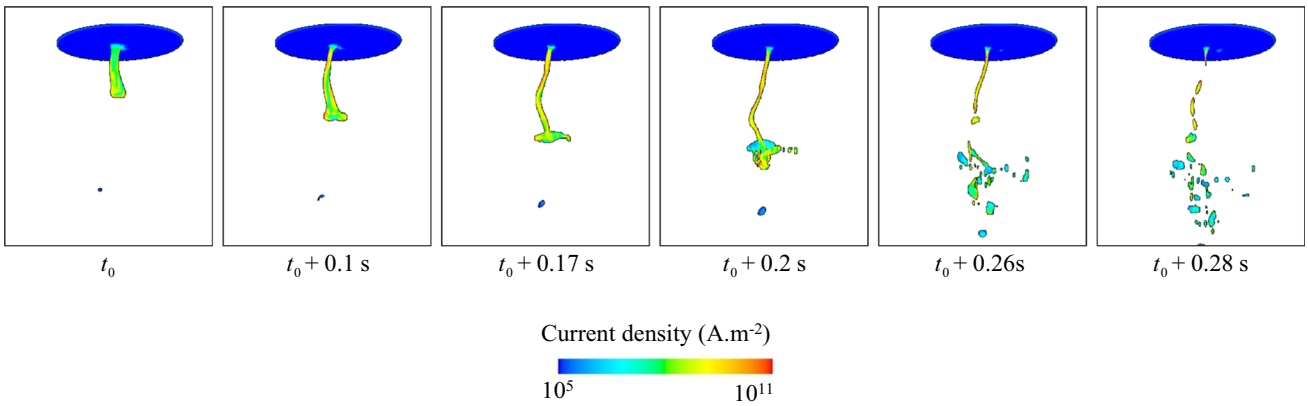

Fig. 8—Atomization of liquid metal faucet under the electrode when the imposed current is suddenly increased by 30 pct starting at t_0. The metal/slag interface is colored with the electric current density (10^5 to 10^{11} A m^{-2}).

the local condition wherever a droplet is being formed, an almost horizontal magnetic field crosses the faucet axis. However, this magnetic field is weak in the center of the electrode and strong at the electrode extremity. The depletion of the droplet observed in the present results can be used to predict that during a large scale process the droplets fall will be deviated toward the center.

During the ESR process, the melting rate is carefully controlled through the power supply system. The control is achieved mainly by adapting the amount of current imposed through the electrode. Complex control algorithms are used in industry. During the process, the imposed current is changed seconds after seconds in a discrete and non-smooth manner. If the imposed vertical current is increased by 30 pct (from 1000 to 1300 A), the Lorenz force can be expected to increase by 70 pct.

In order to simulate such regulation scheme, the applied current was sinusoidally increased within a relatively short time of 0.02 second (50 Hz). This sudden increase of the applied current generates eddy currents within the metal faucet which forces the electric current to flow within a thin layer just near the interface between the slag and the metal. This phenomenon is similar to currents flowing within a skin depth in alternating (AC) current conditions. Locally, the increase in Lorentz force is in fact much larger than 70 pct, and its magnitude and its localization near the surface can

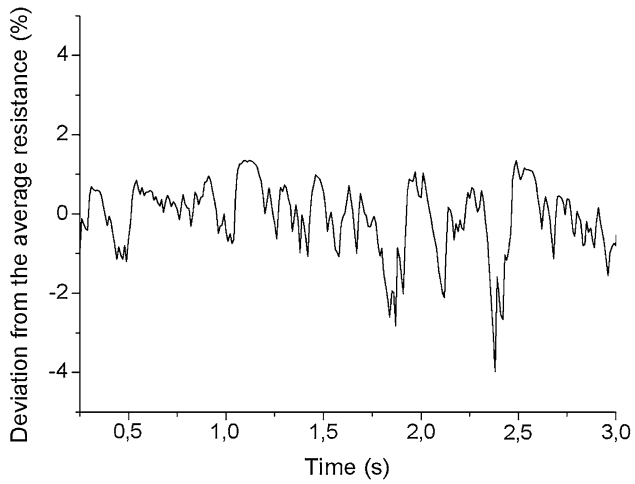

Fig. 9—Fluctuation of the resistance during melting assuming an interface tension of 0.1 N m^{-1}.

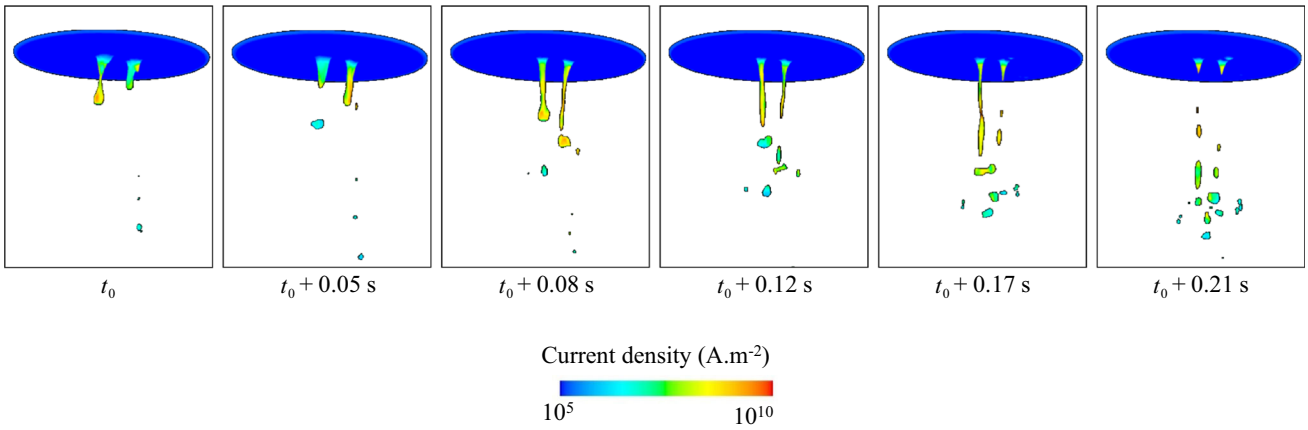

Fig. 10—Droplet formation with small surface tension under the electrode. The metal/slag interface colored with electric current density magnitude (10^5 to 10^{10} A m^{-2}).

explain the flattening of the large droplet as shown in Figure 8. Then, the remaining liquid metal faucet elongates and finally explodes in multiple mini droplets due to electromagnetic pinch effect.

B. *Interfacial tension of 0.1 N m^{-1}*

Properties of slags are known to vary strongly with the proportion of chemical components. From one slag to another, the viscosity or the interface tension can differ by large factors. In addition, strong variations with temperature exist as well. With an interfacial tension of 0.1 N m^{-1}, it can be observed that the computed resistance (Figure 9) does not show the same behavior as that found for a larger surface tension (Figures 5 and 6). The electric resistance is continuously fluctuating but does not exceed 4 pct of the main value. It can be seen that these variations are due to an almost continuous release of small droplets as shown in Figure 10. Here, two to three faucets form and break into droplets of about 0.5 to 4 mm diameter. Due to a difference in the drag force, smaller droplets fall at smaller speed than larger droplets. New droplets depart before even the impact of previous droplets on the slag/pool interface. This quasi continuous presence of droplets in the slag height does not allow the electric current distribution to find a steady state, *i.e.*, the resistance can never reach a constant value as shown in Figure 5. Nevertheless, the peaks corresponding to the lowest value of resistance can still be linked to some relatively large droplets departure (larger than 2 mm).

Since the liquid metal is not concentrated in a unique faucet, the electric current can choose several "metallic paths" to flow downward. Thus, the faucets experience smaller electric current density (max 10^{10} A m^{-2}) than they experienced in the previous case (max 10^{11} A m^{-2}). This means that within the faucet, the actual Lorentz force magnitude is decreased by a factor of 10. In other words, the effective ratio between the electromagnetic force and the interfacial tension force is not different from the case where the surface tension was set to 1 N m^{-1}.

V. CONCLUSIONS

In order to simulate the droplet formation during melting of a metallic electrode, a 3D VOF model was coupled with a magnetohydrodynamic model. The model was applied to the melting of an electrode assuming a small and a large value of the melt/slag interfacial tension. It was shown that with large interfacial tension, only one faucet forms and larger droplets are released. The fluctuation of the resistance can easily be interpreted as lower peaks shown up during the release of each primary or satellite droplets. The resistance decreases with the decrease of the distance between the accumulated liquid metal under the electrode and the slag/pool interface. The minimum value of the resistance is reached at the departure of the first droplet (~1 to 2 cm). Then, a slight increase occurs before a second minimum is reached corresponding to the detachments of a second large droplet. Afterward, some satellite droplets are released, which have smaller electric signature.

Assuming a small interfacial tension, two to three faucets appear from where smaller droplets depart. In this case, the space between the electrode and the liquid pool surface is filled with many small droplets. The continuous release of droplets generates constant electric resistance fluctuations. In this configuration, it is not possible to clearly link the resistance signal with the droplets distribution in the domain.

The effect of applying an external horizontal magnetic field on the behavior of the system is also studied. The applied horizontal magnetic field is an order of magnitude larger than the self-induced magnetic field which is originated from the imposed current. A strong depletion of the droplet toward the mold was predicted when a horizontal magnetic field is applied.

The results of the present DC investigation will be taken as a base for the exploration of melting under AC conditions. If only electrodynamics aspects are considered, the difference between an AC and a DC signal of a droplet fall can be expected to be very small. The only expected effects are related to the possible spreading of

eddy currents generated within the electrode into the slag domain. At 60 Hz, we assume it to be small. However, much larger effects are expected if electrochemical aspects are considered especially for processes operating at low frequency. Some additional efforts must be taken to resolve phenomena in industrial-scale processes. At those scales, it can be expected that a complex coupling between droplets formation, slag/pool interface and electric current exists.

ACKNOWLEDGMENTS

The financial support by the Austrian Federal Ministry of Economy, Family and Youth, and the National Foundation for Research, Technology and Development is gratefully acknowledged.

NOMENCLATURE

L	Length of mold (m)
R_e	Radius of electrode (m)
R_1	Inner radius of mold (m)
R_2	Outer radius of mold (m)
M_R	Melt rate of electrode (kg s^{-1})
I_0	Magnitude of imposed current (A)
f_1	Volume fraction of slag
f_2	Volume fraction of metal
σ	Electric conductivity (Ω^{-1} m^{-1})
σ_1	Electric conductivity of slag (Ω^{-1} m^{-1})
σ_2	Electric conductivity of metal (Ω^{-1} m^{-1})
ρ	Density (kg m^{-3})
ρ_1	Density of slag (kg m^{-3})
ρ_2	Density of metal (kg m^{-3})
μ	Viscosity (kg m^{-1} s^{-1})
μ_1	Viscosity of slag (kg m^{-1} s^{-1})
μ_2	Viscosity of metal (kg m^{-1} s^{-1})
μ_0	Magnetic Permeability constant (J m^{-1} A^{-1})
u	Vector of velocity (m s^{-1})
u_x	Velocity component in x direction (m s^{-1})
u_y	Velocity component in y direction (m s^{-1})
u_z	Velocity component in z direction (m s^{-1})
g	Gravitational constant (m s^{-2})
p	Pressure (Pa)
t	Time (s)
F_L	Lorentz force (N)
j	Current density (A m^{-2})
A	Vector of magnetic potential (V s m^{-1})
A_r	Magnetic potential component in r direction (V s m^{-1})
A_θ	Magnetic potential component in θ direction (V s m^{-1})
A_z	Magnetic potential component in z direction (V s m^{-1})
ϕ	Electric scalar potential (V)
B	Magnetic induction (Tesla)
Res	Electrical resistance (Ω)
δ_{Res}	Deviation from averaged electrical resistance (pct)
τ	Averaging time (s)

REFERENCES

1. J. Campbell: *Metals*, 1970, vol. 20 (7), pp. 23–35.
2. K. Makropoulos and H. Winterhager: *Arch. Eisenhüttenwesen*, 1976, vol. 47, pp. 211–16.
3. Y. Kojima, M. Kato, T. Toyoda, and M. Inouye: *Trans. ISIJ*, 1975, vol. 15, pp. 397–406.
4. B. Korousic: *Arch. Eisenhüttenwesen*, 1976, vol. 47, pp. 283–88.
5. United States Patent 6019811, "Metals Processing Control by Counting Molten Metal Droplets", 2000.
6. M. Murgaš, A.S. Chaus, A. Pokusa, and M. Pokusová: *ISIJ Int.*, 2000, vol. 40 (10), pp. 980–86.
7. T. EI-Gammal and M. Hajduk: *Arch. Eisenhüttenwesen*, 1978, vol. 49, pp. 235–39.
8. A. Kharicha, W. Schützenhöfer, A. Ludwig, R. Tanzer, and M. Wu: *Steel Res. Int.*, 2008, vol. 79, pp. 632–36.
9. A.H. Dilawari and J. Szekely: *Metall. Trans. B*, 1997, vol. 8B (6), pp. 227–36.
10. K.M. Kelkar, J. Mok, S.V. Patankar, and A. Mitchell: *J. Phys. IV Fr.*, 2004, vol. 120, pp. 421–28.
11. A. Jardy, D. Ablitzer, and J.F. Wadier: *Metall. Trans. B*, 1991, vol. 22B, pp. 111–20.
12. M. Choudhary and J. Szekely: *Metall. Trans. B*, 1980, vol. 11B, pp. 439–53.
13. A. Mitchell and G. Beynon: *Metall. Trans. B*, 1971, vol. 2B, pp. 3333–45.
14. A. Kharicha, A. Ludwig, and M. Wu: *Mater. Sci. Eng. A*, 2005, vols. 413–414, pp. 129–34.
15. A. Kharicha, W. Schützenhöfer, A. Ludwig, and G. Reiter: *Mater. Sci. Forum*, 2010, vol. 649, pp. 229–36.
16. A. Kharicha, M. Wu, and A. Ludwig: *ISIJ*, 2014, vol. 54, pp. 1621–28.
17. E. Karimi-Sibaki, A. Kharicha, J. Bohacek, M. Wu, and A. Ludwig: *Metall. Mater. Trans. B*, 2015, vol. 46B, pp. 2049–61.
18. E. Karimi-Sibaki, A. Kharicha, J. Bohacek, M. Wu, and A. Ludwig: *Adv. Eng. Mater.*, 2015, , DOI:10.1002/adem.201500391.
19. O. Biro and K. Preis: *IEEE Trans. Magn.*, 1989, vol. 25 (4), pp. 3145–59.